JAMES | Journal of Advances in Modeling Earth Systems

RESEARCH ARTICLE
10.1029/2019MS001996

Local Grid Refinement in New Zealand's Earth System Model: Tasman Sea Ocean Circulation Improvements and Super-Gyre Circulation Implications

Erik Behrens[1], Jonny Williams[1], Olaf Morgenstern[1], Phil Sutton[1,2], Graham Rickard[1], and Michael J. M. Williams[1]

[1]National Institute of Water and Atmospheric Research (NIWA), Wellington, New Zealand, [2]School of Environment, University of Auckland, Auckland, New Zealand

Key Points:
- NZESM is a nested fully coupled ESM based on UKESM with a high-resolution ocean grid of 1/5° around New Zealand
- The oceanic circulation is improved in NZESM over the nested domain and model biases of temperature and salinity are reduced
- The Super-Gyre intensifies and expands southward due to wind changes triggered by changes in the large-scale heat transport

Supporting Information:
- Supporting Information S1

Correspondence to:
E. Behrens,
erik.behrens@niwa.co.nz

Citation:
Behrens, E., Williams, J., Morgenstern, O., Sutton, P., Rickard, G., & Williams, M. J. M. (2020). Local grid refinement in New Zealand's earth system model: Tasman Sea ocean circulation improvements and super-gyre circulation implications. *Journal of Advances in Modeling Earth Systems*, *12*, e2019MS001996. https://doi.org/10.1029/2019MS001996

Received 17 DEC 2019
Accepted 3 JUN 2020
Accepted article online 9 JUN 2020

Abstract This paper describes the development of New Zealand's Earth System Model (NZESM) and evaluates its performance against its parent model (United Kingdom Earth System Model, UKESM) and observations. The main difference between the two earth system models is an embedded high-resolution (1/5°) nested region over the oceans around New Zealand in the NZESM. Due to this finer ocean model mesh, currents such as the East Australian Current, East Australian Current Extension, Tasman Front, and Tasman Leakage, and their volume and heat transports are better simulated in the NZESM. The improved oceanic transports have led to a reduction in upper ocean temperature and salinity biases over the nested region. In addition, net transports through the Tasman Sea of volume, heat and salt in the NZESM agree better with previously reported estimates. A consequence of the increased cross-Tasman Sea transports in the NZESM is increased temperatures and salinity west of Australia and in the Southern Ocean reducing the meridional sea surface temperature gradient between the subtropics and sub-Antarctic. This also leads to a weakening of the westerly winds between 60°S and 45°S over large parts of the Southern Ocean, which reduces the northward Ekman transport, reduces the formation of Antarctic Intermediate Water, and allows for a southward expansion of the Super-Gyre in all ocean basins. Connecting an improved oceanic circulation around New Zealand to a basin-wide Super-Gyre response is an important step forward in our current understanding of how local scales can influence global scales in a fully coupled earth system model.

Plain Language Summary We describe the model development of the New Zealand Earth System Model and assess its performance against the model on which it is based (United Kingdom Earth System Model) and observations. The New Zealand Earth System Model is a fully coupled earth system model, which aims to model all relevant bio-physical processes in and between the atmosphere, land, ocean, and sea-ice. The main difference between both models is that the oceans around New Zealand in the New Zealand Earth System Model are more precisely modeled, due to a refined ocean model mesh in this region. That results in a more accurate oceanic circulation around New Zealand in the New Zealand Earth System Model compared to the United Kingdom Earth System Model and reduced model biases of temperature and salinity. These oceanic changes have implications beyond the oceans around New Zealand, causing a warming in the Southern Ocean and a related weakening of the westerly winds over the Southern Ocean. This weakening of the winds allows subtropical waters to reach further south into the Southern Ocean. It is notable that regional changes in the ocean circulation can have implications on the global scale.

1. Introduction

New Zealand is a maritime continent, and its weather and climate are directly impacted by the surrounding ocean (Basher & Thompson, 1996; Mullan, 1998). It occupies the intersection between subtropical waters to its north and sub-Antarctic water masses to its south, separated by the Subtropical Front (STF). Due to the prevailing westerly winds, the Tasman Sea and the air-sea fluxes of heat and moisture over this region can be considered a pacemaker for New Zealand's weather and climate. The Tasman Sea is fueled by the East Australian Current (EAC), which transports warm and salty waters from the tropics along the east coast of Australia into the Tasman Sea (Figure 1b). At around 32°S the EAC bifurcates into the EAC-Extension (EAC-Ext), which continues southward, and the Tasman Front (TF), which flows eastward toward New Zealand. The TF is dominated by eddies, particularly in the western Tasman Sea, leading to the suggestion

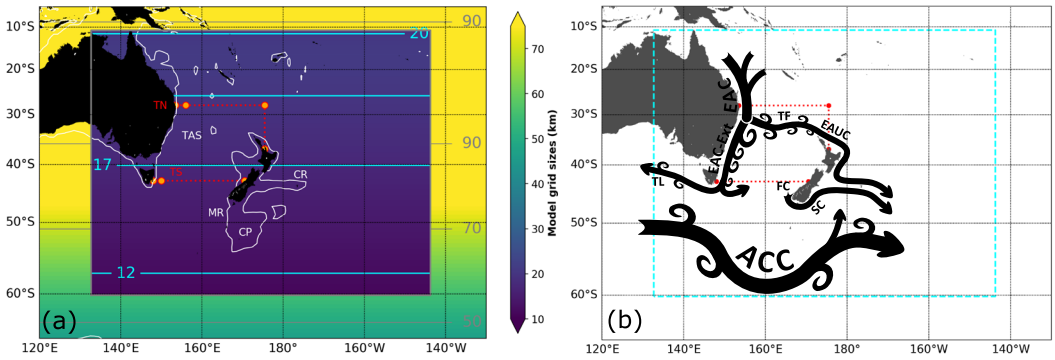

Figure 1. (a) Grid sizes of NZESM in km with high-resolution domain embedded into a global eORCA1 domain are shown by the color shading and contours. Two control sections which run from Australia to New Zealand are shown in by the red dotted lines. The orange dots mark the segments which have been used to calculate transports. The Macquarie Ridge (MR), Campbell plateau (CP), Chatham Rise (CR), Tasman Leakage (TL), Tasman Sea (TAS), Tasman North (TN) section, and Tasman south (TS) section have been labeled. The 1,000 m iso-bath is shown by the white contour. (b) Schematic of major ocean currents in the region: East Australian Current (EAC), East Australian Current extension (EAC-Ext), Tasman Front (TF), East Auckland Current (EAUC), Fiordland Current (FC), Southland Current (SC), and Antarctic Circumpolar Current (ACC).

that it is more accurately described as an eastern EAC-Ext (Oke et al., 2019). While instantaneous fields are dominated by eddies, the TF is clearly visible in temporal means. Because this work uses a model that is eddy-permitting but not eddy-resolving and focuses on interannual time scales, the TF terminology has been used. The EAC-Ext is a region of high mesoscale eddy activity with eddies transporting water from the boundary current into the interior Tasman Sea (Bull et al., 2017; Oliver et al., 2015). A portion of the EAC-Ext leaves the Tasman Sea as the Tasman Leakage (TL) to the Indian Ocean (Rintoul & Bullister, 1999; Speich et al., 2002). This export pathway is part of the Super-Gyre circulation, which connects all three subtropical gyres in the Southern Hemisphere (Cai, 2006). The TF crosses the Tasman Sea and feeds the East Auckland Current (EAUC); the western boundary current on the east coast of the North Island of New Zealand. This current continues south and interacts with a series of standing eddies before following the Chatham Rise into the Pacific Ocean (Chiswell et al., 2015).

The STF is located at around 45°S south of Tasmania and is characterized by strong horizontal gradients in temperature, salinity, and nutrients (Orsi et al., 1995). A weak eastward flow is associated with the STF while crossing the Tasman Sea. The STF is deflected south as it approaches the South Island of New Zealand. The STF forms the Southland Current east of the South Island and then turns east along Chatham Rise.

The interaction of these currents and water masses with the exceptional bathymetry, such as sea-mounts, ridges, and plateaus around New Zealand, makes the oceanic conditions unique and challenging to model and to observe. Long-term oceanographic observations in the region include mooring arrays within the EAC, Expendable Bathythermograph transects between New Zealand, Australia, and Fiji, and dispersed Argo data. Glider missions within the EAC and EAUC are slowly complementing our understanding of the variability of these boundary currents.

Global climate models struggle to precisely simulate the oceanic conditions in this region (Law et al., 2017; Rickard et al., 2016), which has motivated tailored model development such as ACCESS-OM (Bi et al., 2013). Some of the reported model biases of these coupled models can be linked to the relatively coarse oceanic model grids and the inability of these models to precisely simulate western boundary currents and resolve important processes such as mesoscale eddies. To overcome this shortcoming some modeling centers have developed high-resolution configurations for CMIP6 (e.g., Storkey et al., 2018) to incorporate the impact of mesoscale eddies. Such global high-resolution simulations have been shown to reduce some model biases (Muller et al., 2018; Roberts et al., 2016) but require substantially more computational resources. Nested model grids provide an alternative, where areas of interest can be simulated at finer scales and at much lower computational cost. In this paper we describe such a tailored model solution for New Zealand which, together with other model developments, has become known as the New Zealand Earth System Model (NZESM).

The paper is structured as follows. Section 2 provides the model description of NZESM. Section 3 highlights the model performance of NZESM against the United Kingdom Earth System Model (UKESM) and observations, and section 4 provides a discussion and summary.

2. Model Description

NZESM is based on UKESM (see Kuhlbrodt et al., 2018; Sellar et al., 2019; Storkey et al., 2018, for a detailed model description and evaluation): NEMO (Madec, 2008) is used to simulate the ocean physics, CICE (Hunke et al., 2017; Rae et al., 2015) for the sea-ice, the Unified Model (UM) (Walters et al., 2019) for the atmosphere, JULES (Walters et al., 2019) for the land surface, and MEDUSA (Yool et al., 2013) for the ocean biogeochemistry. All model components are coupled together via OASIS-MCT (Craig et al., 2017) to build a fully coupled interactive earth system model (ESM).

The UKESM configuration, where NZESM has been branched off, uses a global 1° tripolar model grid (eORCA1) to simulate the ocean and a N96 grid for the atmosphere. Due to the coarse oceanic grid, mesoscale eddies are not resolved and have been parameterized (Gent & McWilliams, 1990) with a spatially varying coefficient (Held & Larichev, 1996). Isopycnal mixing has been parameterized following Redi (1982). For horizontal viscosity a value of 20,000 m^2/s (Laplacian) and 1,000 m^2/s for isopycnal diffusion has been used. A geothermal heat flux at the ocean floor has been applied to simulate geothermal processes (Goutorbe et al., 2011). NEMO supports local grid refinement capabilities, also known as nesting (Adaptive Grid Refinement In Fortran, AGRIF; Debreu et al., 2008). Here a fine model mesh can be embedded in a coarser ocean model grid via a two-way nesting scheme, allowing for interactive coupling between both model grids, which is known as two-way nesting. Several nested configurations have been previously used to address scientific research questions (Behrens, 2013; Behrens et al., 2012; Biastoch et al., 2008; Schwarzkopf et al., 2019). In the case of the NZESM the nested high-resolution ocean model domain spans from 132.7°E to 143.7°W and 60.17°S to 10.75°S with a nominal resolution of 1/5°, which translates into grid sizes of 12 to 20 km (Figure 1a); this resolution makes the model eddy-permitting around New Zealand. Since the model mesh is largely able to simulate eddies no eddy parameterization has been applied in the high-resolution nest; however, it is still applied to the coarse model grid. The vertical grid, identical between both model grids, uses 75 z-levels, with a 1 m surface layer which increases with depth to up to 200 m in thickness. The model background viscosity and diffusivity for the nested region have been set to bi-Laplacian 5×10^{10} m^2/s and 20,000 m^2/s (Laplacian) respectively, in comparison to 200 and 1,000 m^2/s for the global grid. The time step of the nested domain has been reduced to 900 s compared to 2,700 s for the global model. For compatibility with AGRIF, a linear-free surface has been used instead of a fully free surface as in UKESM. In addition, a climatology of iceberg-related meltwater fluxes, based on UKESM, has been applied instead of the Lagrangian iceberg tracking scheme, due to the incompatibility of the latter with AGRIF. Apart from these two differences the model settings are identical to UKESM. The model results in section 3 show that differences between NZESM and UKESM originate from the presence of the high-resolution nest and can be causally linked. Therefore, we assume that the other differences have a minor impact on the model response.

In this version of NZESM, the coupling with the atmospheric model is accomplished via the global coarse model, which contains the upscaled information of the nested region. The atmospheric model therefore does not experience the directly resolved eddy fluxes of the nested grid.

ESMs are computationally very expensive due to the model components which form an ESM, the long simulations, and the number of simulations (ensemble size). UKESM typically uses 1,261 CPUs in total, where 1,152 (48 × 24) are allocated for the atmosphere, 108 (12 × 9) for the ocean, and one CPU for handling the ocean output (XIOS). The atmosphere includes the physical core, the atmosphere, the atmospheric chemistry, and the land surface interactions. The ocean includes the physical core and ocean biogeochemistry. In this configuration around 7,500 CPU hours are required to simulate one model year. In comparison NZESM uses in total 1,248 CPUs with 1,008 (36 × 28) for the atmosphere, 240 (20 × 12 global and nested model) for the ocean, and one CPU for the ocean output. In this configuration NZESM uses 9,500 CPU hours for one model year, a CPU increase of 25% compared to UKESM.

However, this increase is very small compared to the roughly 300,000 CPU hours which would be required for increased ocean resolution of 0.25° globally, the standard of global high-resolution earth system models.

In other words, NZESM has a higher horizontal oceanic resolution around New Zealand than global high-resolution earth system models and can simulate 31 years for the cost of one global high-resolution ESM year. This is a compelling argument for the development of NZESM, instead of using an off the shelf high-resolution ESMs. For this model comparison paper, we use historical simulations from UKESM and NZESM covering the period from 1950 to 2014, with NZESM initialized with the same start dump of UKESM in 1950. We note that grid refinement has been applied to NEMO to improve ocean physics in the nested region but not to MEDUSA. However, improvements to the ocean physics (e.g., ocean circulation) due to the high-resolution nest will impact MEDUSA on the coarser global grid. These bio-geochemical impacts are out of scope for this work and will be assessed separately.

Modeled temperature and salinity have been compared with data from EN4 (Good et al., 2013) using the Gouretski and Reseghetti (2010) corrected version 4.2.1. Remotely sensed absolute dynamic topography (ADT), a multi-mission altimeter product (Ssalto/Duacs) from Archiving, Validation and Interpretation of Satellite Oceanographic data (AVISO), has been compared to modeled sea surface height (SSH) to characterize near surface circulation and variability. The Ssalto/Duacs altimeter products were produced and distributed by the Copernicus Marine and Environment Monitoring Service (http://www.marine.copernicus.eu).

3. Model Results

3.1. Mean SSH and Variance Field

The mean SSH fields from AVISO, UKESM, and NZESM are shown in Figures 2a–2c. In AVISO the EAC, the EAC-Ext, and the TF are clearly represented by compressed contour lines, which reflect strong surface geostrophic currents. The horizontal gradient over the Tasman Sea is weak, although there is flow associated with the STF in the order of 3 Sv (Stramma et al., 1995). But since the STF in this region is largely density compensated it is not characterized by a large SSH gradient. To the east of New Zealand's North Island, the southward flow associated with the EAUC and East Cape Currents can be seen, with SSH contours turning southward toward the Chatham Rise. South of 50°S the influence of the Antarctic Circumpolar Current (ACC) is visible with large SSH gradients reflecting strong surface currents. The northern portion of the ACC is deflected southward by the presence of Campbell Plateau, before the flow turns northward toward the Chatham Rise, east of Campbell Plateau.

The mean SSH pattern of UKESM does capture the large-scale features seen in AVISO. The EAC and EAC-Ext are too wide and water which enters the TF is carried too far south within the EAC-Ext. That is indicated by a more southern location of the first contour which passes north of the North Cape of New Zealand. The circulation east of New Zealand is reasonably well captured; however, the flow in the ACC is too strong and too zonal compared to AVISO and tends to expand too far northward east of the Campbell Plateau.

The SSH pattern of NZESM is more in agreement with AVISO than UKESM. The width of the EAC is similar to that in AVISO, and the flow pattern of the TF across the Tasman Sea matches AVISO. Flows associated with the ACC now show the meridional diversions as seen in AVISO, west and east of Campbell Plateau. The ACC itself is stronger than in UKESM in some regions, which could be a result of a more realistic and steeper bathymetry in NZESM. The bathymetry in UKESM is smoother, allowing flows to extend over larger regions, compared to steeper bathymetry in NZESM where flows become concentrated and intensified.

SSH variance provides an indirect measure for eddy kinetic energy and is shown in Figures 2d–2f. AVISO exhibits large variability within the EAC, the separation region, and the EAC-Ext. The variability quickly decays away from the Australian coast. Enhanced variability is also present in the ACC, especially in regions where the ACC shows large meridional variability. In UKESM none of this eddy variability is present due to the coarse model grid, which does not allow for mesoscale eddies to be resolved. NZESM, on the other hand, produces a similar SSH variance pattern to AVISO. Large eddy variability is present in the EAC region, particularly near the region where the EAC separates into the EAC-Ext and the TF. NZESM also shows enhanced eddy variability within the same regions of the ACC as AVISO. The NZESM intensities agree well with AVISO within the EAC separation region and are slightly higher in the sub-Antarctic, but variability is too low in the model north of the separation region.

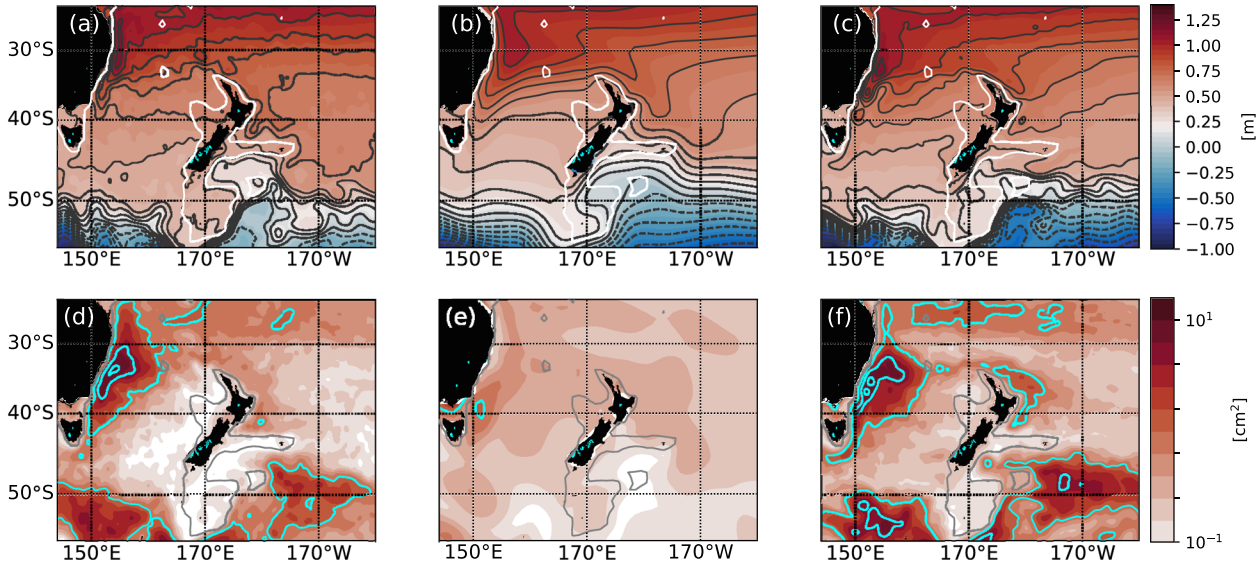

Figure 2. Mean (1995–2014) SSH fields for (a) AVISO, (b) UKESM and (c) NZESM. Contour interval for SSH (black contour lines) is 10 cm. The 1,000 m iso-bath is shown by the white/gray contour line. Variance of SSH for AVISO (d), UKESM (e) and NZESM (f). Contour levels for SSH variance (light blue lines) are 1, 5, 10, and 15 cm^2.

3.2. Mean Cross-Section Properties Along Tasman North

In the following section we describe the differences of temperature, salinity, and cross-section velocity between UKESM, NZESM, and EN4 across two sections which bound the Tasman Sea (Figure 1a). The Tasman North (TN) section cuts through the warm water pathway into the Tasman Sea running across 28°S from Australia to 178°E before turning south with an end point near Auckland. This section characterizes how both models capture the inflow of warm and salty subtropical water into the Tasman Sea, how this water recirculates within the subtropical gyre, or leaves the Tasman Sea as part of the TF and EAUC. Previous studies have shown that net transports across this section control water mass properties in the central Tasman Sea and therefore are of particular interest (Behrens et al., 2019).

The UKESM and NZESM temperature fields are similar (Figures 3a and 3d) with the warmest water found near Australia as part of the EAC inflow and the temperatures cooler moving east along the TN section. The difference between NZESM and UKESM shows that temperatures in NZESM are about 0.5°C warmer in the top 250 m, except for the EAC (Figure 3g). Below 500 m temperatures in NZESM are in general around 0.5° colder than UKESM, except near the boundaries where temperatures are up to 1°C warmer. The comparison to EN4 suggests (supporting information Figure S1) that the temperature biases along this section are reduced in NZESM compared to UKESM. The top 250 m in UKESM along the entire section are around 1°C too cold, while the layer down to 1,200 m is up to 1.5° too warm compared to EN4 (Figure S1d). The UKESM bias shows the opposite pattern to the difference between NZESM-UKESM (Figure 3g) which consequently results in a reduced model bias in NZESM (Figure S1e). The temperature differences between NZESM and UKESM near the coast can be attributed to changes in the boundary currents between both models. Here the EAC, TF, and EAUC become narrower and flow stronger in NZESM with accompanied changes in the baroclinicity.

The salinity field shows three different vertical layers (Figures 3b and 3e), with high salinity in the top 500 m, which is linked to water with subtropical origin. Below this surface layer a fresher layer between 500 and 1,250 m of AAIW is visible, and saltier waters underneath associated with Pacific Deep Waters (PDW). The difference between NZESM and UKESM (Figure 3h) highlights that salinity in NZESM is in general fresher in the upper 1,250 m, but the boundary currents and PDW layer are saltier. Both models present a fresh bias in the top 1,200 m compared to EN4 along this section (Figure S2), and this fresh bias becomes larger in NZESM due to lower but more realistic volume transports of the TF and EAUC, carrying less salty water from the EAC along this pathway.

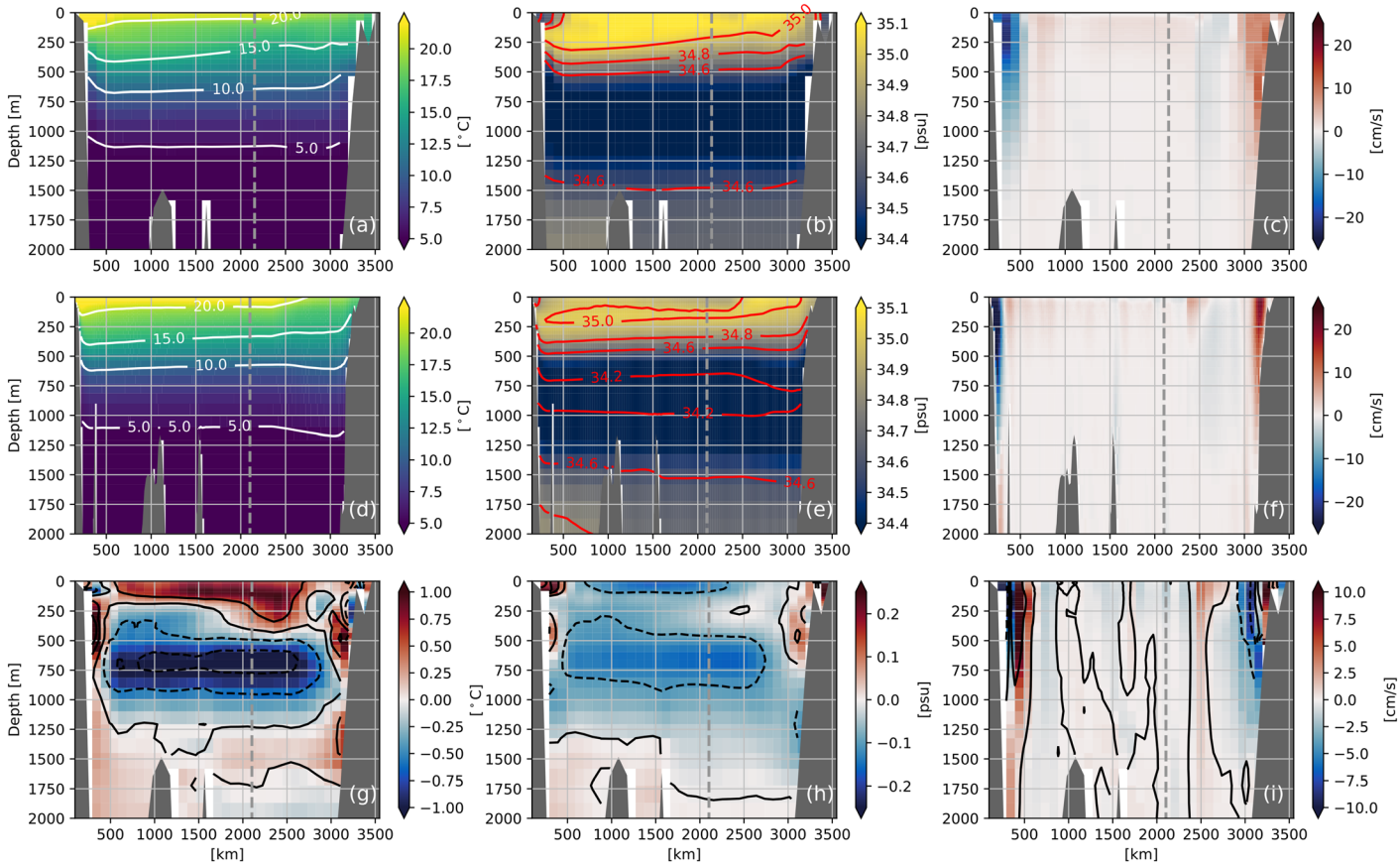

Figure 3. Mean properties (1995–2014) along the Tasman North section. (a, d) Temperature, (b, e) salinity, and (c–f) cross-section velocity for UKESM (top row) and NZESM (middle row). The difference (NZESM minus UKESM) is shown in the bottom row. Temperature contour interval is 5°C. The contour interval for salinity is 0.2 psu. The gray dashed line marks the point where the section turns from zonal to meridional. Contour interval for temperature difference is 0.5°C, for salinity 0.1 psu, and 5 cm/s for cross-section velocities.

The cross-section velocities show that with increasing model resolution the boundary currents become narrower and more intense (Figures 3c and 3f). The EAC extends up to 500 km off the coast in UKESM, while in NZESM it is only 250 km. The same behavior is visible for the EAUC and in the difference between NZESM minus UKESM (Figure 3i).

The differences in temperature and salinity seen along the TN section between both models can be largely explained by large-scale changes in the Super-Gyre Circulation with it extending southward in NZESM. This is discussed in detail in section 3.7. As a consequence of this expansion the top 250 m become warmer and fresher in NZESM. The freshening is counterintuitive but a result of the substantial fresh bias north of the TN (see section 3.5) which extends in NZESM further into the Tasman Sea. The expansion of the Super-Gyre Circulation also affects the volume transports of EAC-Ext, TF, EAUC, and throughflow through the Tasman Sea. In NZESM all of these transports are closer to observational estimates compared to UKESM (Table 1). The throughflow in UKESM is close to zero (−0.33 Sv) while in NZESM −4.82 Sv is being transported through the Tasman Sea. Therefore, more heat and salt are carried through the Tasman Sea southward in NZESM, rather than being advected north of New Zealand within the overly strong TF in UKESM. The cross-section velocity anomalies (Figure 3i) suggest baroclinic changes in the boundary currents, which lead to nonuniform anomalies in temperature and salinity over the water column.

3.3. Mean Cross-Section Properties Along Tasman South

The TS section runs from Tasmania to the South Island along 43°S. This section characterizes the southern boundary of the Tasman Sea with the Tasman Outflow transporting water toward the Indian Ocean. Along the TS section the impact of changes in throughflow through the Tasman Sea between UKESM and NZESM

Table 1
Time Mean (1995–2014) Transports

	Observations	UKESM	NZESM
EAC volume transport	−25 to −37 Sv (Ridgway & Dunn, 2003); −22 Sv (Mata et al., 2000); −22 Sv (Sloyan et al., 2016)	−28.7 Sv ± 5.7	−16.8 Sv ± 7.8
EAC-Ext volume transport	−19 Sv (Ridgway & Dunn, 2003)	−7.1 Sv ± 4.0	−8.8 Sv ± 11.9
TF volume transport	13 Sv (Ridgway & Dunn, 2003) 8 Sv (Stanton, 2010)	21.8 Sv ± 4.8	9.5 Sv ± 6.8
TL volume transport	−8 Sv (Stephen R. Rintoul & Sokolov, 2001); −8 Sv (Ridgway & Dunn, 2007)	−8.0 Sv ± 5.2	−10.6 Sv ± 8.8
Cross-Tasman Sea volume transport	−7.4 Sv (Ridgway & Dunn, 2003); −9 Sv (Ridgway & Godfrey, 1994); −3 to −8 Sv (Hill et al., 2011)	−0.33 ± 4.8	−4.82 ± 6.8
Cross-Tasman Sea Heat transport		-24×10^{12} J/s ± 181×10^{12}	-320×10^{12} J/s ± 279×10^{12}
Cross-Tasman Sea FW transport		0.01 Sv ± 0.04	−0.07 Sv ± 0.05
ITF transport	15 Sv (Gordon et al., 2010)	15.3 Sv ± 2.7	14.8 Sv ± 2.5
STG Pacific Ocean 153°E to 173°E, 37.5°S to 20°S		−43.9 Sv ± 4.6	−45.4 Sv ± 12.7
STG Indian Ocean 23°W to 53°W, 45°S to 20°S	−41 to −58 Sv (Palmer et al., 2004)	−94.1 Sv ± 3.9	−96.6 Sv ± 3.9
STG Atlantic Ocean −57°W to 27°W, 45°S to 20°S		−49.5 Sv ± 6.3	−51.3 Sv ± 6.9

Note. The Cross-Tasman Sea transports are defined as the net transports of volume, heat, and freshwater across the TS section (Figure 1a). A references salinity of 34.8 has been used to compute freshwater (FW) transports. The strengths for the Subtropical Gyres (STG) in each ocean basin are provided. Modeled STG strengths are computed from minimum barotropic stream function over the regions provided in the table. The standard deviations for the modeled transport are provided based on monthly mean values.

become more obvious than across the TN section (Figure 4). NZESM is substantially warmer over the entire section, with differences compared to UKESM reaching up to 2°C in the top 750 m in the central Tasman Sea (Figure 4g). This is due to the combined impact of the NZESM resolving EAC-Ext eddies, which carry warm and salty waters from the boundary current (EAC-Ext) into the interior Tasman Sea and enhanced southward transport through the Tasman Sea. UKESM displays over large parts of this section a cold temperature bias in the order of −1°C within the top 500 m compared to EN4 (Figure S3). This bias turns positive in NZESM in the order of 0.5°C (Figure S3e).

The salinity differences in the top 750 m are very coherent with the temperature differences, with salinity being up to 0.5 psu saltier in the NZESM compared to the UKESM (Figure 4h). This supports our conclusion about increased southward volume, heat, and salt transport, as part of the Super-Gyre extension and a more unstable EAC-Ext in NZESM.

However, the AAIW layer becomes fresher (750–1,750 m), which can be a consequence of enhanced AAIW production or a surface freshening or a surface warming in the formation region, following the concepts developed by Bindoff and McDougall (1994). However, the positive temperature anomalies at the same depth range conflicts with enhanced AAIW production rates and surface warming. Results in section 3.7 suggest that a surface freshening in combination with reduced AAIW are likely the reasons for the observed anomalies.

In UKESM the EAC-Ext and the TL extends up to 750 km into the Tasman Sea, compared with only 250 km in NZESM (Figures 4c–4f). In general, NZESM shows more meridional structures than UKESM over the section. Near the New Zealand shelf a southward flow is visible, the Fiordland Current (Chandler et al., 2019), which contributes to the STF. This current is more prominent and wider in NZESM and barely recognizable in UKESM.

3.4. Mean Properties in the Tasman Sea

The TN and TS sections enclose a large portion of the Tasman Sea, where we compare the mean temperature and salinity profiles against the EN4 dataset for the upper 1,000 m where the differences are largest (Figures 5a and 5b). The mean profiles for the Tasman Sea are shown by the solid lines, and the shading indicates the minimum and maximum range over the period 2004–2014.

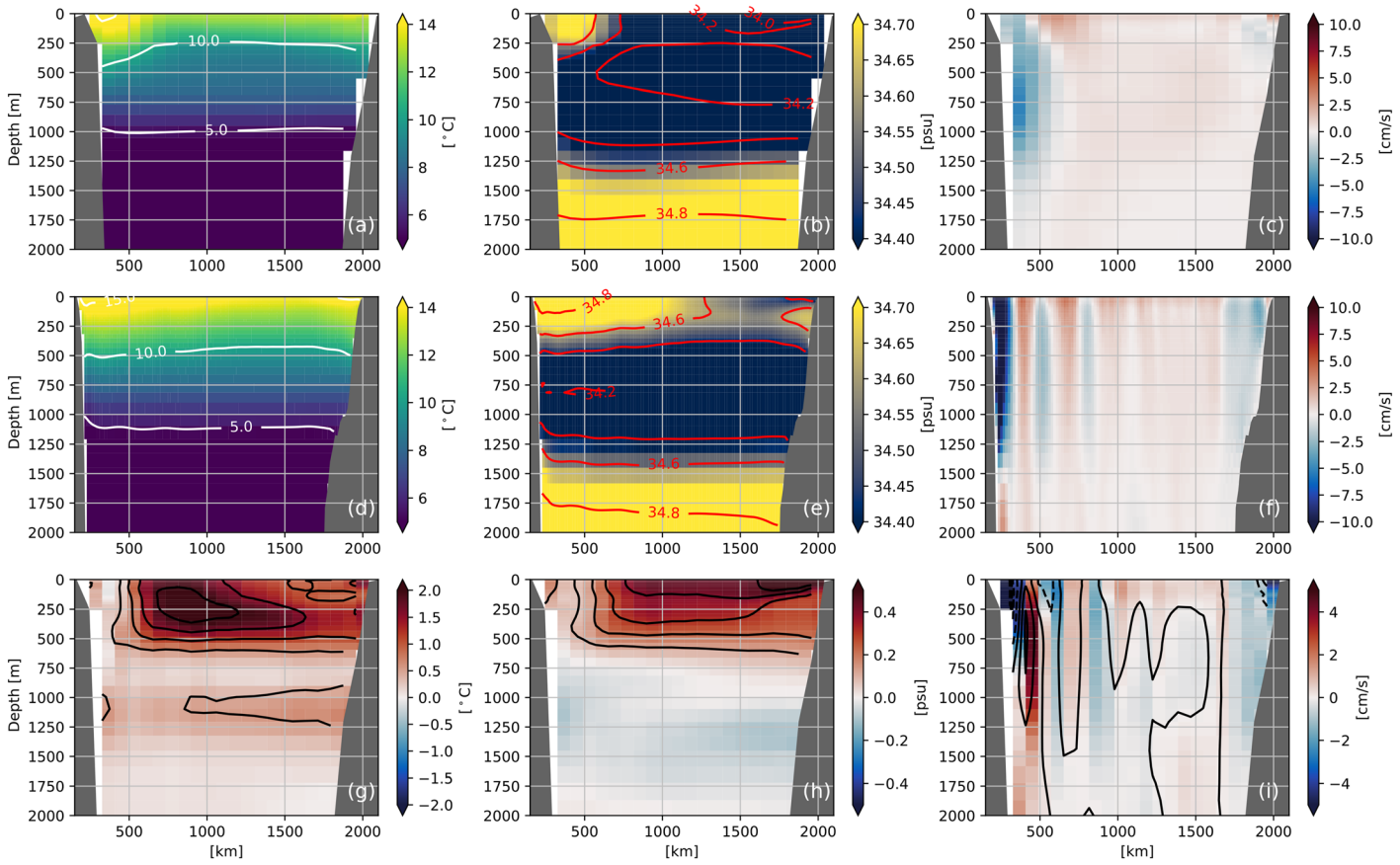

Figure 4. Mean properties (1995–2014) along the Tasman South section. (a, d) Temperature, (b, e) salinity, and (c–f) cross-section velocity for UKESM (top row) and NZESM (middle row). The difference between NZESM minus UKESM is shown in the bottom row. Temperature contour interval is 5°C. The contour interval for salinity is 0.2 psu. Contour interval for temperature difference is 0.5°C, for salinity 0.1 psu, and 5 cm/s for cross-section velocities.

For temperature in the top 50 m, UKESM is around 1°C cooler compared to the EN4 mean profile and the minimum values (Figure 5a). Here NZESM shows a better match with EN4 with only small differences. Between 100 and 600 m NZESM is around 0.8°C cooler than EN4, while UKESM shows a close match with EN4.

Salinities in both models are too fresh compared to EN4. Differences reach up to 0.8 psu in the upper 200 m of the water column and decrease to 0.2 psu at 1,000 m (Figure 5b). In NZESM the salt bias is reduced in the top 700 m by around 0.2 to 0.6 psu. UKESM shows a large range of around ±0.2 psu within the top 200 m, while the range of EN4 and NZESM is smaller at around ±0.1 psu. The reason for the overall fresh bias of both models is connected to the general precipitation surplus compared to observations over most of the Pacific and Indian Ocean (Sellar et al., 2019). However, overall the top 100 m temperatures in NZESM are improved, while the substantial salinity difference over the top 1,000 m remains and is only slightly reduced in NZESM.

Due to the large biases in both models the density and density structure is affected (Figure 5c). Here, both models present water masses which are too light compared to EN4 in particular near the surface. Despite this shortcoming of both models, the profile structure compares reasonably between both models and EN4, within NZESM is capturing it better than UKESM.

The interannual variability and long-term changes of these temperature and salinity profiles are shown in Figures 6 and 7. Note in panels (a) and (b) of each figure the seasonal cycle of UKESM has been removed. UKESM shows a positive temperature trend over the entire period of about 1.2°C/decade (top 1,000 m), consistent with the increasing CO_2 concentrations (Figure 6a). The largest warming occurs in the top 400 m of the water column. Most of the interannual variability in the order of ±0.5°C is constrained to this layer too.

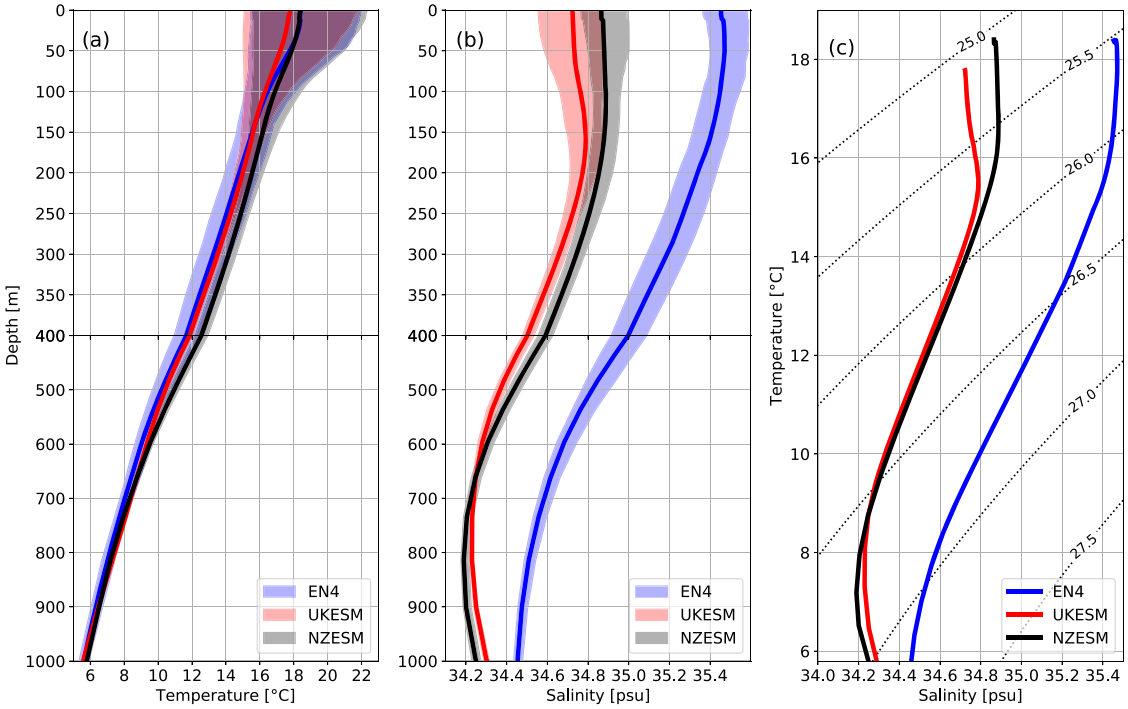

Figure 5. Vertical mean (2004–2014) profiles for (a) temperature, (b) salinity averaged over the Tasman Sea for EN4, UKESM, and NZESM shown as solid lines. Note that the depth scale in (a) and (b) is not equidistant. The shading represents the minimum and maximum range over the 20-year period. (c) Temperature-salinity plot for the three datasets from (a) and (b). The dashed contour lines show potential density in kg/m^3.

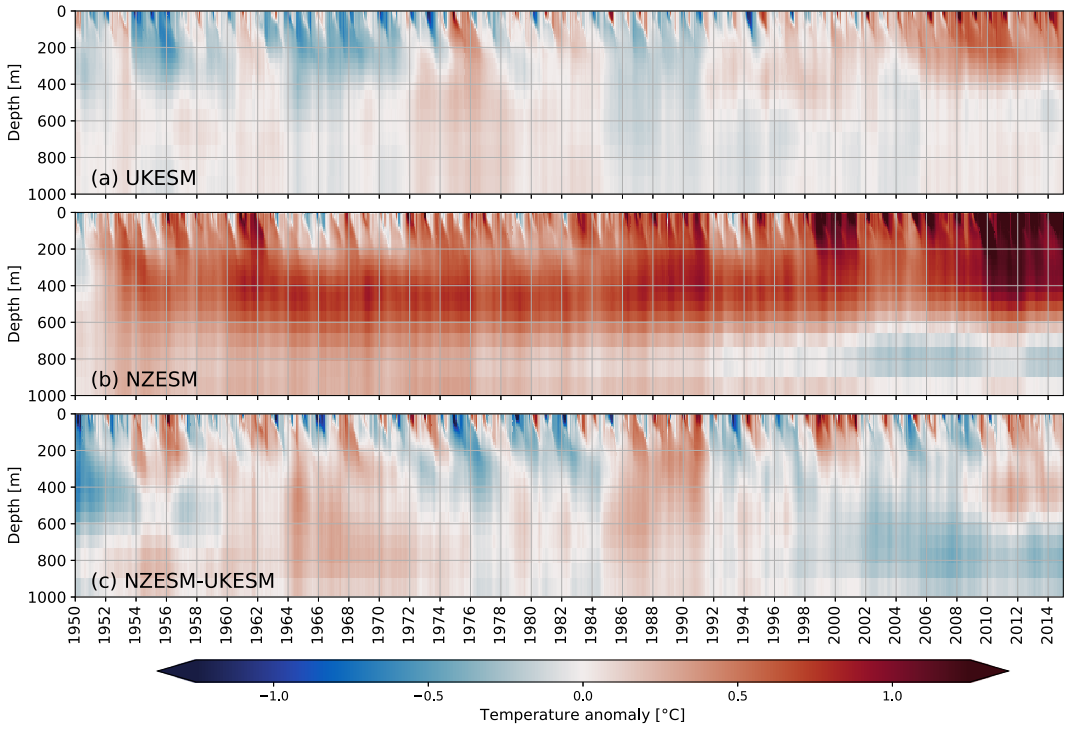

Figure 6. Temporal evolution of the mean temperature anomalies in the Tasman Sea for (a) UKESM, (b) NZESM, and (c) NZESM minus UKESM. In (a) and (b) the seasonal cycle from UKESM has been subtracted to illustrate the transition from the joint restart. In (c) the individual seasonal cycles have been removed before computing the anomalies to highlight the changes in interannual variability between UKESM and NZESM.

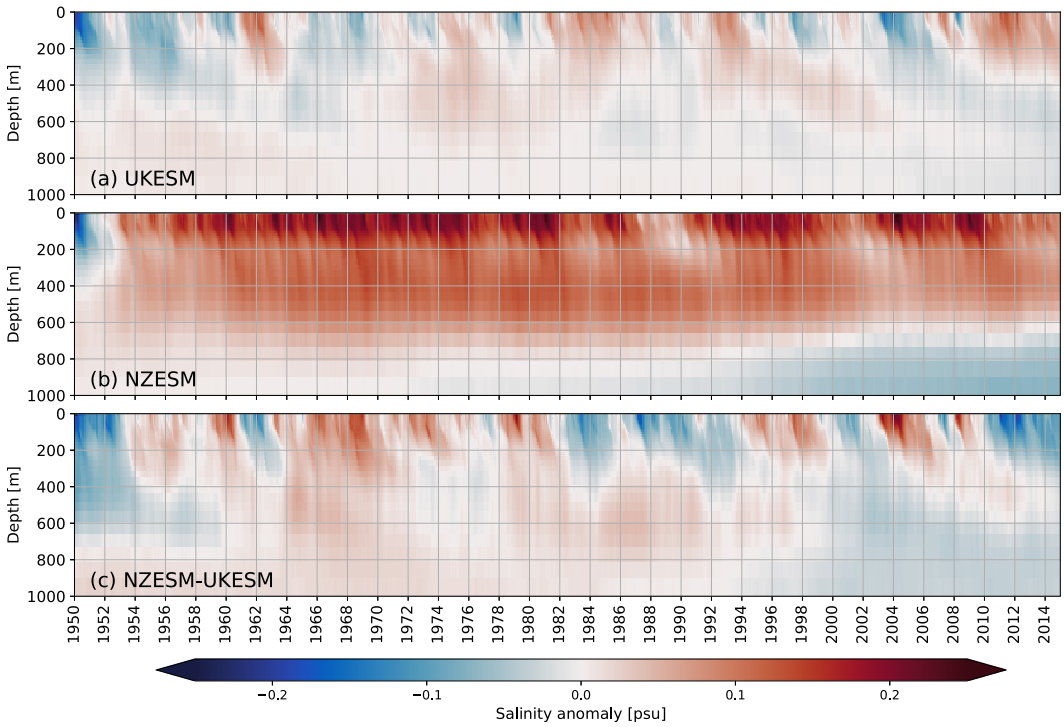

Figure 7. Temporal evolution of the mean salinity anomalies over the Tasman Sea for (a) UKESM, (b) NZESM, and (c) NZESM minus UKESM. In (a) and (b) the seasonal cycle from UKESM has been subtracted to illustrate the transition from the joint restart. In (c) the individual seasonal cycles have been removed before computing the anomalies to highlight the changes in interannual variability between UKESM and NZESM.

NZESM presents a fast adjustment (~5 year) to warmer temperatures of about +0.5°C in the upper 1,000 m from the joint restart with UKESM. The largest warming occurs within the top 600 m of the water column. Superimposed on this warming is a very similar long-term warming trend in the top 400 m as that seen in UKESM (Figure 6b). However, the layer between 600 and 800 m exhibits a cooling of around −0.2°C, which was not present in UKESM. In addition to the cooling trend, the interannual variability differs between both models despite the same starting point (Figure 6c). That suggests that due to ocean–atmosphere feedbacks the large-scale climate pattern and associated variability have been impacted due to the presence of the high-resolution nest in NZESM.

Salinity in UKESM shows two opposing trends (Figure 7a). The top 600 m becomes saltier (0.1 psu/decade), while the layer between 600 and 1,000 m becomes fresher (−0.06 psu/decade). The salinity in NZESM adjusts within the first 5 years from the joint starting point with UKESM as for temperature (Figure 7b). The top 100 m shows the largest salinity increase of about 0.2 psu which decreases with depth. Only little change is seen below 800 m, with freshening trends in NZESM slightly larger (−0.13 psu/decade) for 600–1,000 m compared to UKESM. Salinity also shows changes to the interannual variability (Figure 7c). We note that interannual temperature and salinity variability do not necessary co-vary.

3.5. Surface Temperature and Salinity Biases

After having presented the localized impacts on the Tasman Sea, we show the regional changes around New Zealand due to the presence of the high-resolution nest in NZESM.

Surface temperature and salinity biases of UKESM and NZESM are shown in Figure 8. UKESM shows a general cold bias exceeding −0.5°C north of ~35°S. The EAC-Ext is too warm, while the remaining Tasman Sea is more than −1°C too cold. To the east of New Zealand we observe a dipole pattern with a positive bias northeast of Chatham Rise and a negative bias southeast of it. In the ACC region the biases tend to be positive, with biases exceeding 2°C east of 150°E. In comparison to UKESM, in NZESM the cold model bias north of New Zealand in the subtropical region is reduced. The Tasman Sea changes from a large negative to small positive model bias in the order of 0.2°C. In addition, the model biases east of New Zealand have also been reduced in NZESM in both size and intensity. The only region where model biases have become

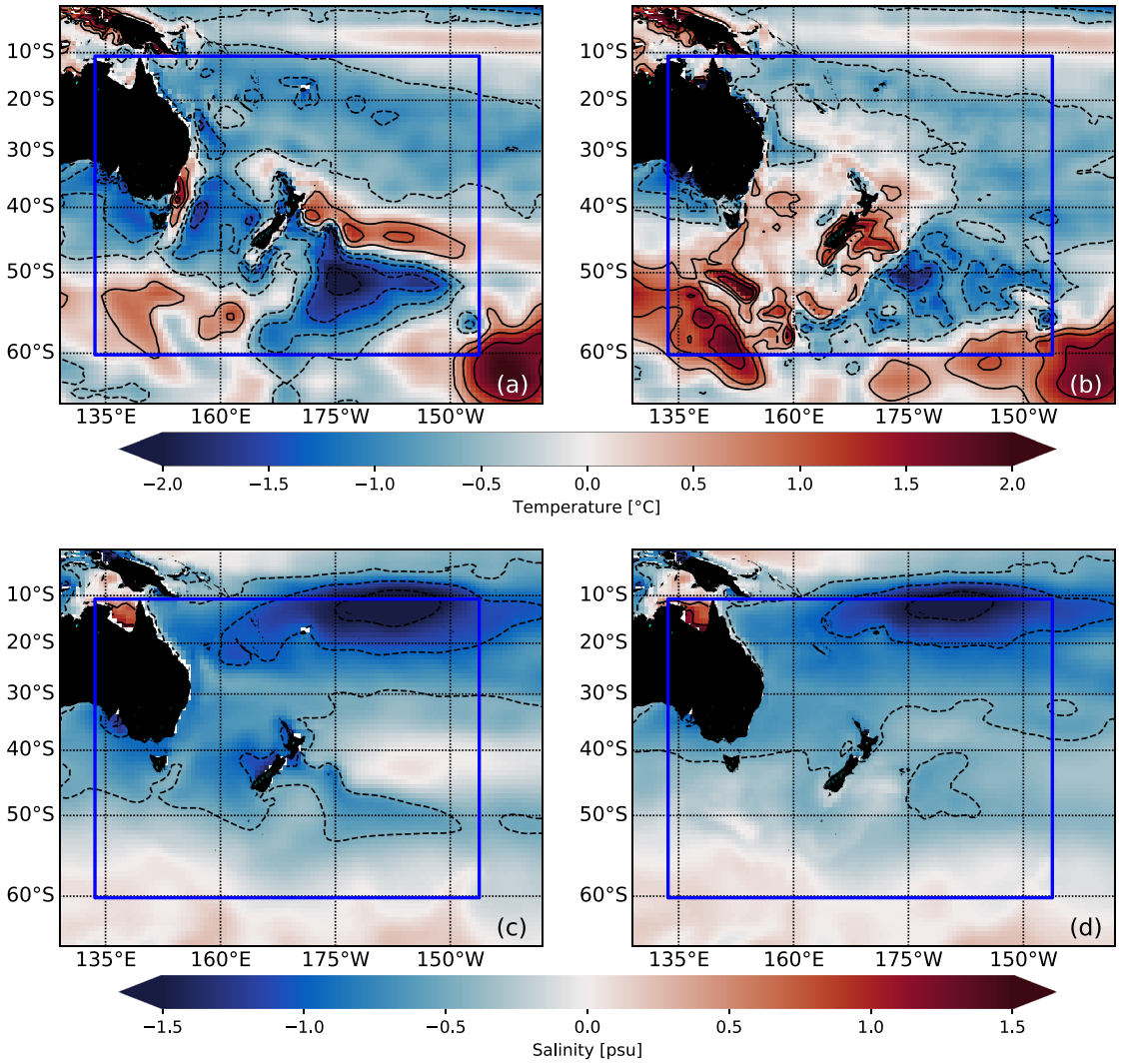

Figure 8. Surface model biases 1995–2014, compared to EN4. (a) SST UKESM, (b) SST NZESM, (c) SSS UKESM, and (d) SSS NZESM. The dark blue box marks the region of the high-resolution nest. Contour interval for temperature is 0.5°C and 0.5 psu for salinity.

larger are in the Australian sector south of 50°S, where previously positive biases of 0.5°C now exceed 1.5°C. This warming is consistent with the temperature anomalies shown across the TS section, Figure 4.

UKESM has an overall negative surface salinity bias in the subtropical region. The SSS bias exceeds −1.5 psu around 10°S, 160°W. The negative bias becomes weaker when moving south until it turns positive between 55°S and 60°S. Over the Tasman Sea the bias is between −0.6 and −0.7 psu. In NZESM the fresh bias is reduced in most regions and values in the Tasman Sea are close to −0.5 psu, while values along the TN section have increased slightly.

Some of the changes in the model biases between UKESM and NZESM can be attributed to changes in the oceanic circulation in NZESM. As presented earlier, NZESM transports more heat into and through the Tasman Sea, which results in warmer SSTs and reduces the overall negative SST bias in this region. In combination with an enhanced salt transport into and through the Tasman Sea in NZESM, the warmer SST increases evaporation which causes a further reduction of the negative SSS bias.

3.6. Advective Response of Top 500 M Temperature and Salinity Anomalies

In this section we seek to highlight the advective response of the nested region in NZESM, due to changes in volume, heat, and freshwater transports. These changes, in combination with atmospheric feedbacks, trigger

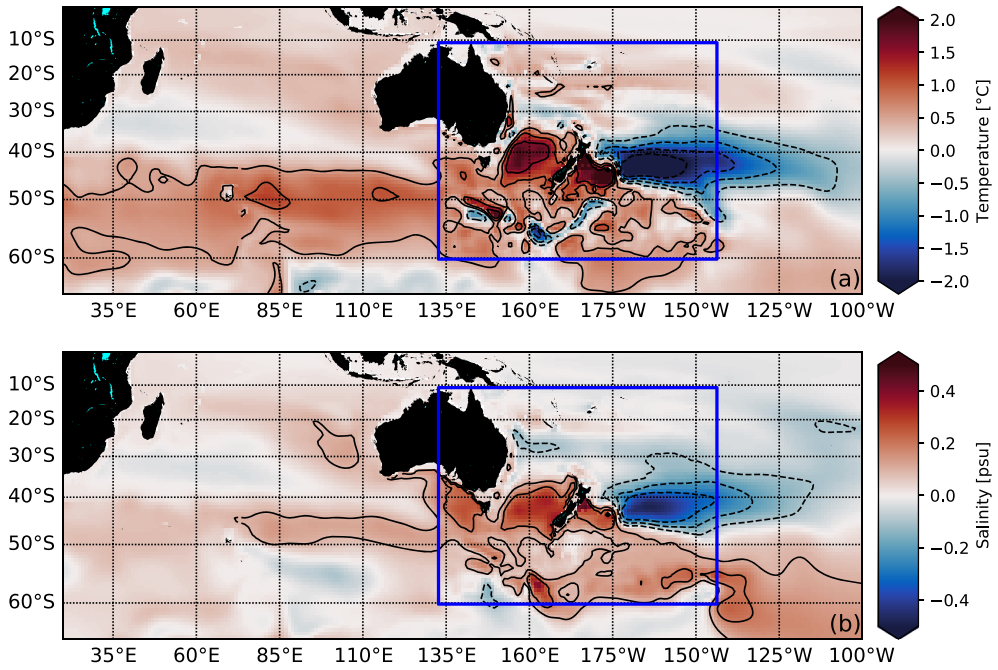

Figure 9. Mean (1995–2014) top 500 m a temperature and b salinity difference: NZESM minus UKESM. The dark blue box marks the region of the high-resolution nest. Contour interval for temperature is 0.5°C and 0.5 psu for salinity.

responses far beyond the boundaries of the nested high-resolution domain. Here we present the mean temperature and salinity differences over the top 500 m between NZESM and UKESM (Figure 9). In these depth-averaged differences, the response due to ocean advection is dominant over changes in the surface fluxes of heat and freshwater.

The largest impact occurs inside the boundaries of the nested region, confirming that differences between NZESM and UKESM are mainly driven by the presence of the high-resolution nest in NZESM. In NZESM the Tasman Sea is around 1.5°C warmer compared to UKESM. This anomaly extends into the Indian Ocean sector between 60°S and 40°S, over the Chatham Rise and southeast into the Southern Ocean. To the east of Chatham Rise a large negative anomaly exceeding 2°C has developed, which extends further into the Pacific Ocean.

The main anomaly pattern can be attributed to the changes in the oceanic circulation in NZESM. As described in sections 3.2 and 3.3, the southward cross-Tasman Sea transport of heat is increased in NZESM compared to UKESM. This change in heat advection between NZESM and UKESM causes the positive temperature difference in the Tasman Sea, the south Indian Ocean, and the Chatham Rise. In UKESM most of this heat is carried instead through the Tasman Sea by the overly strong TF and EAUC to the east of New Zealand. In NZESM this heat pathway is reduced due to a more realistic transport of the TF and causes the negative anomalies in this region. The positive temperature differences west of Australia are a result of the increased TL transport of heat and feeds into the northern branch of the Indian Subtropical Gyre (van Sebille et al., 2012).

Salinity shows a very similar difference pattern to temperature, where positive differences span from the Tasman Sea into the South Indian and South Pacific Ocean. The good match to the temperature differences suggest that most of these anomalies are caused by changes in the ocean advection of heat and freshwater, rather than by regional changes in the surface fluxes.

3.7. Impacts on the Super-Gyre Circulation

As seen in the previous sections, the differences are not restricted to the nested regions and have far-reaching impacts due to advective processes and atmospheric feedbacks. This can impact the basin-scale circulation including the Super-Gyre circulation, which connects all three subtropical gyres in the southern

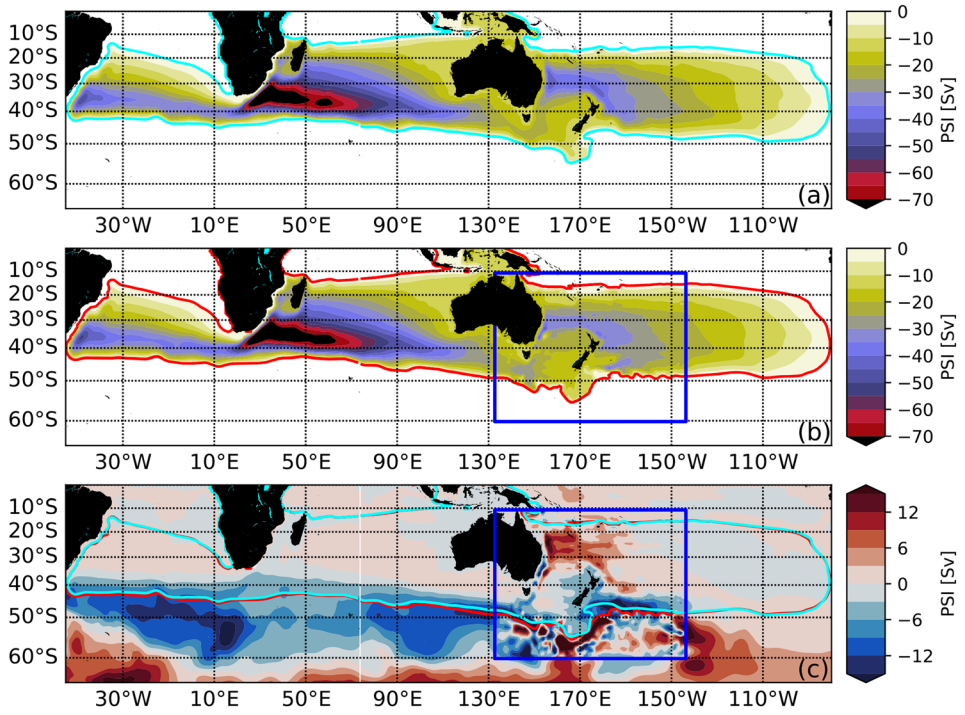

Figure 10. Time mean (1995–2014) barotropic stream function for (a) UKESM and (b) NZESM and (c) difference (NZESM minus UKESM). Blue (red) contour shows 0 Sv contour for UKESM (NZESM). The nested region is shown by the blue box.

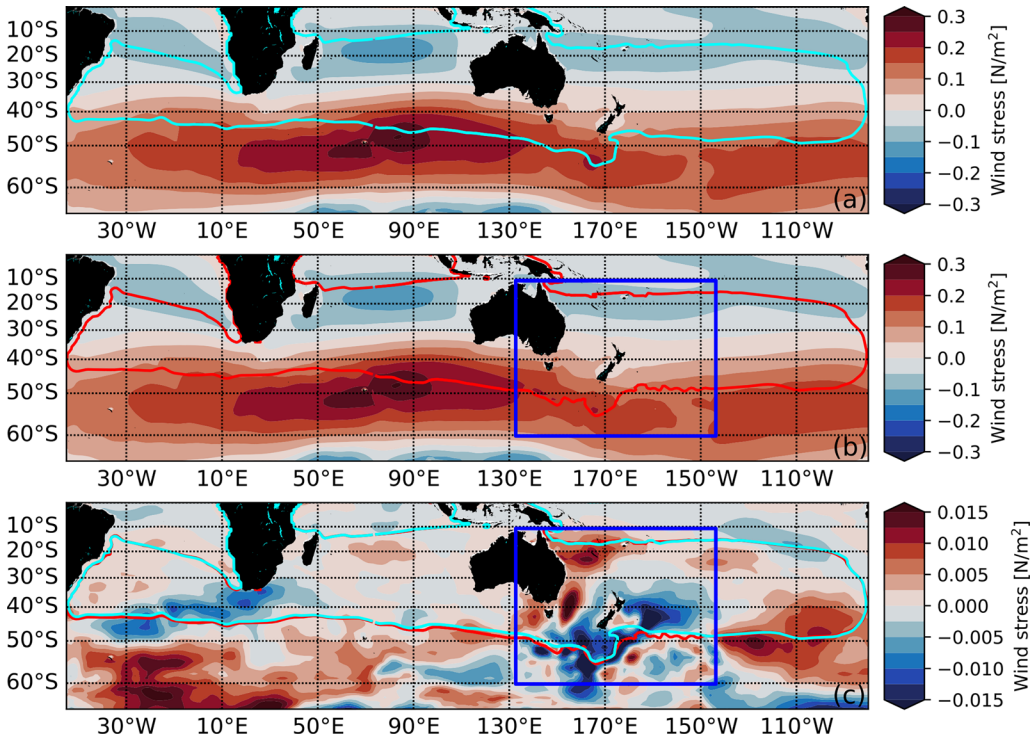

Figure 11. Time mean (1995–2014) zonal wind stress (a) UKESM and (b) NZESM and (c) difference between NZESM minus UKESM. The nested region is shown by the red box. The zero Sverdrup contour line of the barotropic stream function of UKESM (cyan) and NZESM (red) is overlaid. The nested region is shown by the dark red box.

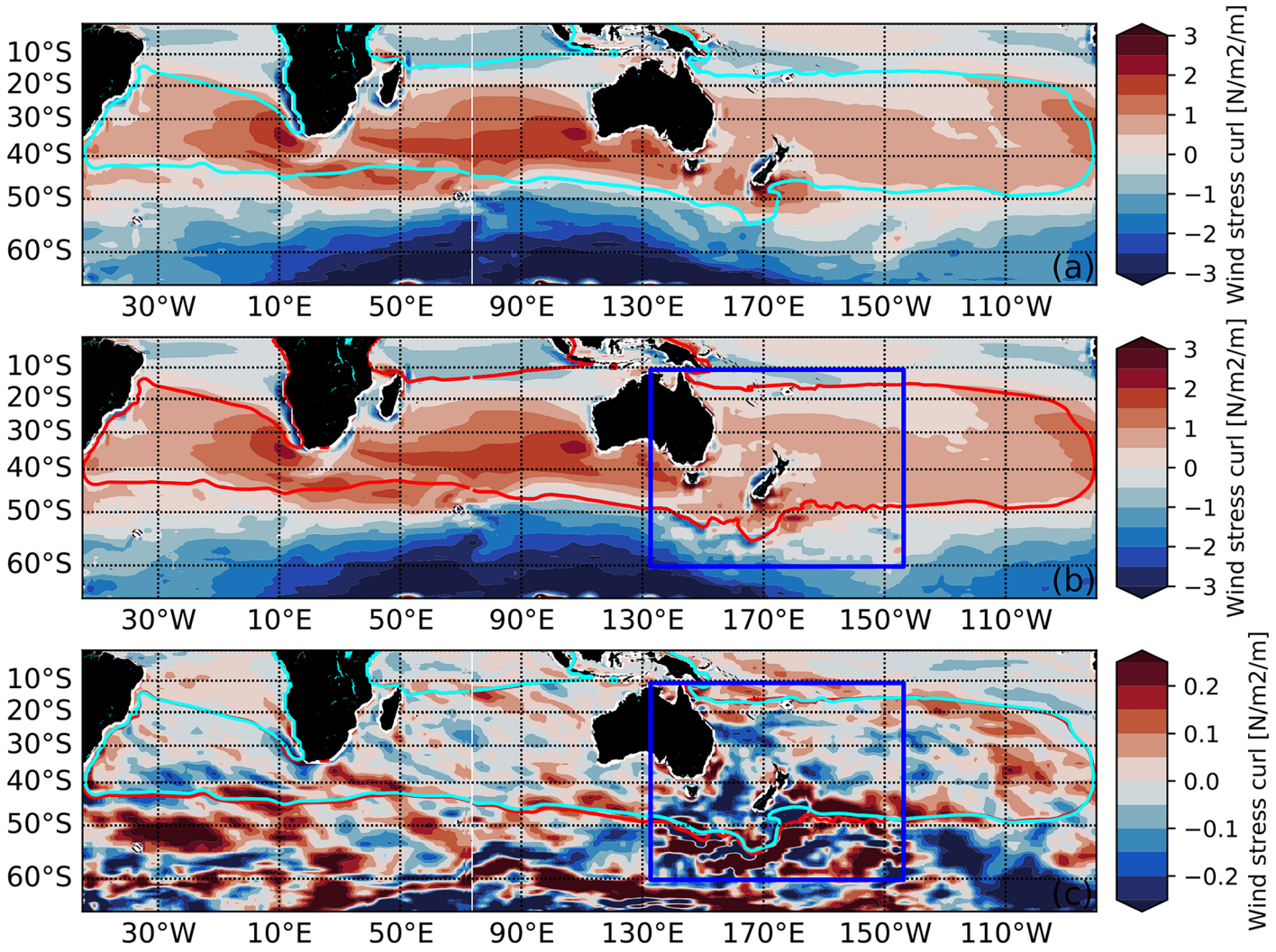

Figure 12. Time mean (1995–2014) wind stress curl for (a) UKESM and (b) NZESM and (c) difference between NZESM minus UKESM. Values have been scaled by 1×10^7. The nested region is shown by the red box. The zero Sverdrup contour line of the barotropic stream function of UKESM (cyan) and NZESM (red) is overlaid. The nested region is shown by the black box.

hemisphere (Cai, 2006; Ridgway & Dunn, 2007; Speich et al., 2007). The barotropic stream function for UKESM and NZESM and the difference are shown in Figure 10, highlighting the Super-Gyre circulation and the inter-basin connectivity. The 0 Sv contour is shown for UKESM and NZESM to define the gyre boundaries. All three subtropical gyres are visible in UKESM and NZESM, with centers near the western boundary due to the western intensification. The barotropic stream function difference shows a strengthening for all three gyres centers of 2–4 Sv (see Table 1). Over the nested region we see a weakening of the circulation north of New Zealand (positive anomalies) of about 8 Sv, which reflects weaker transports of the TF in NZESM compared to UKESM. This large-scale weakening in combination with changes in the heat transport explains the negative temperature anomalies in the TN section at depths between 500 and 1,000 m and are not driven by changes in the AAIW formation. Along Campbell Plateau and Chatham Rise we see enhanced circulation, which is reflected by negative (positive) anomalies north (south) of the Super-Gyre boundary.

In addition to the enhanced Super-Gyre circulation, a slight southward expansion of the gyre boundary is visible in most regions in the Southern Ocean. The southward expansion is caused by reduced zonal wind stress south of the Super-Gyre boundary between 60°S and 45°S by about 5–10% (Figure 11) in NZESM compared to UKESM. The exception is the Indian Ocean sector where zonal winds increase. The overall

reduction in zonal winds leads to a weakening of northward Ekman transport and allows for a southward expansion of the Super-Gyre. The reduction in Ekman transport causes a weakening of AAIW formation, which was seen in the TS section (section 3.3 and Figure 4) by positive temperature anomalies in the AAIW depth range (1,000–1,250 m). The related slightly negative salinity anomalies suggest in addition a freshening of the source waters, which is supported by the negative anomalies in Figure 9 around 60°S–65°S south of Australia and New Zealand.

Lastly, the intensification of the individual subtropical gyre transports is due to positive wind stress curl anomalies over the gyre centers (Figure 12) on the western side of each basin. This results in a speed up of gyre circulation in each basin via the Sverdrup circulation.

4. Conclusions and Discussion

NZESM is a fully coupled earth system model based on UKESM (Kuhlbrodt et al., 2018). This paper describes the model development of NZESM and evaluates its model performance against UKESM and observations. The main enhancement of NZESM compared with UKESM is an embedded high-resolution (1/5°) nested ocean around New Zealand. This has been accomplished through local grid refinement techniques using AGRIF (Debreu et al., 2008) with a two-way nesting scheme, which allows for a smooth transition of signals between the nested grid and the global coarse 1° ocean grid.

The comparison between NZESM and UKESM and observations shows that, due to the finer model mesh in NZESM, the oceanic circulation in the nested region has been improved compared to UKESM. Volume transports of the EAC, EAC-Ext, TF, and TL in NZESM agree better with observed values. Here, UKESM overestimates transports of the EAC and TF by up to a factor of two and underestimates transport of the EAC-Ext. Transports of these currents in NZESM do not differ more than 15% from the observed values. This improvement is mainly achieved through a better representation of the boundary currents, which are too wide in UKESM, and a more realistic bifurcation of the EAC into the EAC-Ext and TL. Here mesoscale eddies play an important role and NZESM simulates the eddy field in the bifurcation region better than UKESM.

The improved separation into the EAC-Ext and TL in NZESM has consequences for the cross-Tasman Sea transport. In UKESM the net volume, heat, and salt transport through the Tasman Sea is too low compared to previous estimates. In NZESM these transports are within the range of those estimates and lead to a reduction of model biases in temperature and salinity in this region.

UKESM shows a large-scale cold (~1–2°C) and fresh (~0.7 psu) bias at the surface around New Zealand. These biases are reduced to nearly zero (±0.2°C) for temperature and ~0.5 psu for salinity. Since the temperature biases are small and do not show a similar pattern to the fresh biases, we conclude that an excess of precipitation and not a lack of evaporation is the main cause for the remaining fresh bias. Reasons remain unknown and are beyond the scope of this ocean-focused study.

Due to ocean advection and atmospheric feedbacks in combination with the two-way nesting, the impact of the high-resolution region propagates well beyond the nest boundaries. The enhanced transport of heat and salt within the TL and through the Tasman Sea causes temperature and salinity to increase along the west coast of Australia and in the upper 500 m of the Southern Ocean.

The SST increase has atmospheric implications too, since it reduces the large-scale meridional SST gradient between subtropical and subpolar regions. That, in turn, weakens the westerlies following the thermal wind equation. This weakening of westerlies is observed in a meridional band between 45°S to 60°S and reduces the northward Ekman transport and causes the Super-Gyre to extend further into the Southern Ocean.

The southward extension has also been recognized in UKESM when comparing the low-resolution version, based on a global 1° (eORCA1) ocean grid, with a high-resolution version based on a global 0.25° (eORCA025) ocean grid (Sellar et al., 2019). These results confirm our hypothesis and findings that the expansion is related to the improved transports of the boundary currents, as seen in NZESM. However, the expansion of the Super-Gyre in UKESM (eORCA025) results in larger SST and sea-ice biases in the Southern Ocean compared with the lower resolution (eORCA1) configurations. In this respect, the performance of UKESM (eORCA1) is better due to a cancelation of errors, which is to some extent linked to the

impact of mesoscale eddies in this region. The UKESM (eORCA025) model grid does not fully resolve eddies in the Southern Ocean, while they are parametrized in the UKESM (eORCA1) configuration. Trying to shed light into the impact of eddies in the Southern Ocean and their regional impact is an active and complex field of research (Doddridge et al., 2019; Hogg et al., 2013; Meredith, 2016), and nesting provides a potential way forward (Patara et al., 2016) to improve our understanding.

The Super-Gyre expansion in NZESM goes along with a gyre circulation intensification of around 2–4 Sv, as a consequence of increased wind stress curl over the individual subtropical gyre centers via the Sverdrup balance. Both the expansion and extension of the Super-Gyre have various ramifications; such as the transport of salt from the Indian to the Atlantic Ocean via the Agulhas Leakage. This has far-reaching consequences for the Atlantic Meridional Overturning Circulation as well as the circulation and sea-ice in the Southern Ocean. Although we observe changes in those quantities, causal links all the way from oceanic changes around New Zealand beyond the Super-Gyre scale are not trivial to establish and are beyond the scope of this paper. The bio-geochemical implications of improvements in the ocean physics around New Zealand are also excluded here.

We have demonstrated with the development of NZESM that we can reduce model biases around New Zealand by embedding a high-resolution ocean nest in a global, relatively coarse resolution earth system model, with a feasible computational cost to allow for a sequence of simulations. The oceanic circulation around New Zealand is more precisely captured in NZESM than without this high-resolution focal region in UKESM. With this step forward, we speculate that climate projections and climate variability modeled by NZESM will be more precise and accurate than without this tailored model development for the New Zealand region.

Data Availability Statement

The model output of NZESM (u-bl274 MetOffice identifier) and UKESM (u-bm456 MetOffice identifier) used for the manuscript is publicly available via Zenodo (http://doi.org/10.5281/zenodo.3581390 and http://doi.org/10.5281/zenodo.3581410). The model code for NZESM (NEMO+CICE) is publicly available online (https://doi.org/10.5281/zenodo.3873691). The EN4 is publicly available from https://www.metoffice.gov.uk/hadobs/en4/download%2010en4%20102%20101.html (Good et al., 2013).

Acknowledgments
This paper obtained funding and support through the Ministry of Business Innovation and Employment Deep South National Science Challenge projects (C01X1412) and Royal Society Marsden Fund (NIW1701). We would like to acknowledge the NeSI High Performance Computing Facility team for their technical support. In addition, we would like to acknowledge the technical guidance of Jérôme Chanut (IPSL, France), Pat Hyder (MetOffice, UK), Jan Harlaβ (GEOMAR, Germany), Torge Martin (GEOMAR, Germany), and the support of Frances Boyson and my son with this project. Furthermore, we acknowledge the time, effort, and constructive comments of all three reviewers to help us improve our manuscript.

References

Basher, R. E., & Thompson, C. S. (1996). Relationship of air temperatures in New Zealand to regional anomalies in sea-surface temperature and atmospheric circulation. *International Journal of Climatology*, *16*(4), 405–425.

Behrens, E. (2013). The oceanic response to Greenland melting: The effect of increasing model resolution. Retrieved from http://macau.uni%2010kiel.de/receive/dissertation_diss_00013684

Behrens, E., Fernandez, D., & Sutton, P. (2019). Meridional oceanic heat transport influences marine heatwaves in the Tasman Sea on interannual to decadal timescales. *Frontiers in Marine Science*, *6*, 228. https://www.frontiersin.org/articles/10.3389/fmars.2019.00228/abstract

Behrens, E., Schwarzkopf, F. U., Lbbecke, J. F., & Bning, C. W. (2012). Model simulations on the long-term dispersal of 137 Cs released into the Pacific Ocean off Fukushima. *Environmental Research Letters*, *7*(3), 034004. https://doi.org/10.1088/1748-9326/7/3/034004

Bi, D. H., Marsland, S. J., Uotila, P., O'Farrell, S., Fiedler, R., Sullivan, A., et al. (2013). ACCESS-OM: The ocean and sea-ice core of the ACCESS coupled model. *Australian Meteorological and Oceanographic Journal*, *63*(1), 213–232. https://doi.org/10.22499/2.6301.014

Biastoch, A., Boning, C. W., & Lutjeharms, J. R. (2008). Agulhas leakage dynamics affects decadal variability in Atlantic overturning circulation. *Nature*, *456*(7221), 489–492. https://www.ncbi.nlm.nih.gov/pubmed/19037313, https://doi.org/10.1038/nature07426

Bindoff, N. L., & McDougall, T. J. (1994). Diagnosing climate change and ocean ventilation using hydrographic data. *Journal of Physical Oceanography*, *24*(6), 1137–1152. https://doi.org/10.1175/1520-0485%281994%29024%3C1137%3ADCCAOV%3E2.0.CO%3B2

Bull, C. Y. S., Kiss, A. E., Jourdain, N. C., England, M. H., & van Sebille, E. (2017). Wind forced variability in eddy formation, eddy shedding, and the separation of the east Australian current. *Journal of Geophysical Research: Oceans*, *122*, 9980–9998. https://doi.org/10.1002/2017JC013311

Cai, W. (2006). Antarctic ozone depletion causes an intensification of the Southern Ocean super-gyre circulation. *Geophysical Research Letters*, *33*, L03712. https://doi.org/10.1029/2005GL024911

Chandler, M., Bowen, M., & Smith, R. O. (2019). The Fiordland current, Southwest New Zealand: Mean, variability, and trends. *New Zealand Journal of Marine and Freshwater Research*, 1–21. https://doi.org/10.1080/00288330.2019.1629467

Chiswell, S. M., Bostock, H. C., Sutton, P. J. H., & Williams, M. J. M. (2015). Physical oceanography of the deep seas around New Zealand: A review. *New Zealand Journal of Marine and Freshwater Research*, *49*(2), 286–317. https://doi.org/10.1080/00288330.2014.992918

Craig, A., Valcke, S., & Coquart, L. (2017). Development and performance of a new version of the OASIS coupler, OASIS3-MCT_3.0. *Geoscientific Model Development*, *10*(9), 3297–3308.

Debreu, L., Vouland, C., & Blayo, E. (2008). AGRIF: Adaptive grid refinement in Fortran. *Computers & Geosciences*, *34*(1), 8–13.

Doddridge, E. W., Marshall, J., Song, H., Campin, J. M., Kelley, M., & Nazarenko, L. (2019). Eddy compensation dampens Southern Ocean sea surface temperature response to westerly wind trends. *Geophysical Research Letters*, *46*, 4365–4377. https://doi.org/10.1029/2019GL082758

Gent, P. R., & McWilliams, J. C. (1990). Isopycnal mixing in ocean circulation models. *Journal of Physical Oceanography*, *20*(1), 150–155.
Good, S. A., Martin, M. J., & Rayner, N. A. (2013). EN4: Quality controlled ocean temperature and salinity profiles and monthly objective analyses with uncertainty estimates. *Journal of Geophysical Research: Oceans*, *118*, 6704–6716. https://doi.org/10.1002/2013JC009067
Gordon, A. L., Sprintall, J., van Aken, H. M., Susanto, D., Wijffels, S., Molcard, R., et al. (2010). The Indonesian throughflow during 2004-2006 as observed by the INSTANT program. *Dynamics of Atmospheres and Oceans*, *50*(2), 115–128. https://doi.org/10.1016/j.dynatmoce.2009.12.002
Gouretski, V., & Reseghetti, F. (2010). On depth and temperature biases in bathythermograph data: Development of a new correction scheme based on analysis of a global ocean database. *Deep Sea Research Part I: Oceanographic Research Papers*, *57*(6), 812–833. https://www.sciencedirect.com/science/article/pii/S0967063710000671, https://doi.org/10.1016/j.dsr.2010.03.011
Goutorbe, B., Poort, J., Lucazeau, F., & Raillard, S. (2011). Global heat flow trends resolved from multiple geological and geophysical proxies. *Geophysical Journal International*, *187*(3), 1405–1419. https://doi.org/10.1111/j.1365-246X.2011.05228.x
Held, I. M., & Larichev, V. D. (1996). A scaling theory for horizontally homogeneous, baroclinically unstable flow on a beta plane. *Journal of the Atmospheric Sciences*, *53*(7), 946–952. https://doi.org/10.1175/1520-0469%281996%29053%3C0946%3AASTFHH%3E2.0.CO%3B2
Hill, K. L., Rintoul, S. R., Ridgway, K. R., & Oke, P. R. (2011). Decadal changes in the South Pacific western boundary current system revealed in observations and ocean state estimates. *Journal of Geophysical Research*, *116*, C01009. https://doi.org/10.1029/2009JC005926
Hogg, A. M., Meredith, M. P., Chambers, D. P., Abrahamsen, E. P., Hughes, C. W., & Morrison, A. K. (2013). Recent trends in the Southern Ocean eddy field. *Journal of Geophysical Research: Oceans*, *120*, 257–267. https://doi.org/10.1002/2014JC010470
Hunke, E., Lipscomb, W., Jones, P., Turner, A., Jeffery, N., & Elliott, S. (2017). CICE, the Los Alamos Sea ice model. In.
Kuhlbrodt, T., Jones, C. G., Sellar, A., Storkey, D., Blockley, E., Stringer, M., et al. (2018). The low-resolution version of HadGEM3 GC3.1: Development and evaluation for global climate. *Journal of Advances in Modeling Earth Systems*, *10*, 2865–2888. https://doi.org/10.1029/2018MS001370
Law, C. S., Rickard, G. J., Mikaloff-Fletcher, S. E., Pinkerton, M. H., Behrens, E., Chiswell, S. M., & Currie, K. (2017). Climate change projections for the surface ocean around New Zealand. *New Zealand Journal of Marine and Freshwater Research*, *52*(3), 309–335. https://doi.org/10.1080/00288330.2017.1390772
Madec, G. (2008). NEMO the ocean engine. *Tech. Rep., Notes de l'IPSL, 27*(1288–1619), 193.
Mata, M. M., Tomczak, M., Wijffels, S., & Church, J. A. (2000). East Australian current volume transports at 30°S: Estimates from the World Ocean circulation experiment hydrographic sections PR11/P6 and the PCM3 current meter array. *Journal of Geophysical Research*, *105*(C12), 28,509–28,526. https://doi.org/10.1029/1999JC000121
Meredith, M. P. (2016). Understanding the structure of changes in the Southern Ocean eddy field. *Geophysical Research Letters*, *43*, 5829–5832. https://doi.org/10.1002/2016GL069677
Mullan, A. B. (1998). Southern hemisphere sea-surface temperatures and their contemporary and lag association with New Zealand temperature and precipitation. *International Journal of Climatology*, *18*(8), 817–840.
Muller, W. A., Jungclaus, J. H., Mauritsen, T., Baehr, J., Bittner, M., Budich, R., et al. (2018). A higher-resolution version of the max Planck institute earth system model (MPI-ESM 1.2-HR). *Journal of Advances in Modeling Earth Systems*, *10*, 1383–1413. https://doi.org/10.1029/2017MS001217
Oke, P. R., Pilo, G. S., Ridgway, K., Kiss, A., & Rykova, T. (2019). A search for the Tasman front. *Journal of Marine Systems*, *199*, 103217. https://doi.org/10.1016/j.jmarsys.2019.103217
Oliver, E. C. J., O'Kane, T. J., & Holbrook, N. J. (2015). Projected changes to Tasman Sea eddies in a future climate. *Journal of Geophysical Research: Oceans*, *120*, 7150–7165. https://doi.org/10.1002/2015JC010993
Orsi, A. H., Whitworth, T., & Nowlin, W. D. (1995). On the meridional extent and fronts of the Antarctic circumpolar current. *Deep-Sea Research Part I-Oceanographic Research Papers*, *42*(5), 641–673. https://doi.org/10.1016/0967-0637(95)00021-W
Palmer, M. D., Bryden, H. L., Hirschi, J., & Marotzke, J. (2004). Observed changes in the South Indian Ocean gyre circulation, 1987–2002. *Geophysical Research Letters*, *31*, L15303. https://doi.org/10.1029/2004GL020506
Patara, L., Boening, C. W., & Biastoch, A. (2016). Variability and trends in Southern Ocean eddy activity in 1/12° ocean model simulations. *Geophysical Research Letters*, *43*, 4517–4523. https://doi.org/10.1002/2016GL069026
Rae, J. G. L., Hewitt, H. T., Keen, A. B., Ridley, J. K., West, A. E., Harris, C. M., et al. (2015). Development of the global sea ice 6.0 CICE configuration for the Met Office global coupled model. *Geoscientific Model Development*, *8*(7), 2221–2230. https://doi.org/10.5194/gmd-8-2221-2015
Redi, M. H. (1982). Oceanic isopycnal mixing by coordinate rotation. *Journal of Physical Oceanography*, *12*(10), 1154–1158. https://doi.org/10.1175/1520-0485%281982%29012%3C1154%3AOIMBCR%3E2.0.CO%3B2
Rickard, G. J., Behrens, E., & Chiswell, S. M. (2016). CMIP5 earth system models with biogeochemistry: An assessment for the Southwest Pacific Ocean. *Journal of Geophysical Research: Oceans*, *121*, 7857–7879. https://doi.org/10.1002/2016JC011736
Ridgway, K. R., & Dunn, J. R. (2003). Mesoscale structure of the mean east Australian current system and its relationship with topography. *Progress in Oceanography*, *56*(2), 189–222. https://doi.org/10.1016/S0079-6611(03)00004-1
Ridgway, K. R., & Dunn, J. R. (2007). Observational evidence for a Southern Hemisphere oceanic supergyre. *Geophysical Research Letters*, *34*, L13612. https://doi.org/10.1029/2007GL030392
Ridgway, K. R., & Godfrey, J. S. (1994). Mass and heat budgets in the east Australian current: A direct approach. *Journal of Geophysical Research*, *99*(C2), 3231. https://doi.org/10.1029/93JC02255
Rintoul, S. R., & Bullister, J. L. (1999). A late winter hydrographic section from Tasmania to Antarctica. *Deep-Sea Research Part I-Oceanographic Research Papers*, *46*(8), 1417–1454. https://doi.org/10.1016/S0967-0637(99)00013-8
Rintoul, S. R., & Sokolov, S. (2001). Baroclinic transport variability of the Antarctic circumpolar current south of Australia (WOCE repeat section SR3). *Journal of Geophysical Research*, *106*(C2), 2815–2832. https://doi.org/10.1029/2000JC900107
Roberts, M. J., Hewitt, H. T., Hyder, P., Ferreira, D., Josey, S. A., Mizielinski, M., & Shelly, A. (2016). Impact of ocean resolution on coupled air-sea fluxes and large-scale climate. *Geophysical Research Letters*, *43*, 10,430–10,438. https://doi.org/10.1002/2016GL070559
Schwarzkopf, F. U., Biastoch, A., Böning, C. W., Chanut, J., Durgadoo, J. V., Getzlaff, K., et al. (2019). The INALT family—A set of high-resolution nests for the Agulhas Current system within global NEMO ocean/sea-ice configurations. *Geoscientific Model Development*, *12*(7), 3329–3355. https://doi.org/10.5194/gmd-12-3329-2019
Sellar, A. A., Jones, C. G., Mulcahy, J. P., Tang, Y., Yool, A., Wiltshire, A., et al. (2019). UKESM1: Description and evaluation of the UK earth system model. *Journal of Advances in Modeling Earth Systems*, *11*, 4513–4558. https://doi.org/10.1029/2019MS001739
Sloyan, B. M., Ridgway, K. R., Cowley, R., Sloyan, B. M., Ridgway, K. R., & Cowley, R. (2016). The east Australian current and property transport at 27°S from 2012 to 2013. *Journal of Physical Oceanography*, *46*(3), 993–1008. https://doi.org/10.1175/JPO-D-15-0052.1

Speich, S., Blanke, B., & Cai, W. J. (2007). Atlantic meridional overturning circulation and the Southern Hemisphere supergyre. *Geophysical Research Letters*, *34*, L23614. https://doi.org/10.1029/2007GL031583

Speich, S., Blanke, B., de Vries, P., Drijfhout, S., Ds, K., Ganachaud, A., & Marsh, R. (2002). Tasman leakage: A new route in the global ocean conveyor belt. *Geophysical Research Letters*, *29*(10), 1416. https://doi.org/10.1029/2001GL014586

Stanton, B. R. (2010). An oceanographic survey of the Tasman front. *New Zealand Journal of Marine and Freshwater Research*, *15*(3), 289–297. https://doi.org/10.1080/00288330.1981.9515924

Storkey, D., Blaker, A. T., Mathiot, P., Megann, A., Aksenov, Y., Blockley, E. W., et al. (2018). UK Global Ocean GO6 and GO7: A traceable hierarchy of model resolutions. *Geoscientific Model Development*, *11*(8), 3187–3213. https://doi.org/10.5194/gmd-11-3187-2018

Stramma, L., Peterson, R. G., & Tomczak, M. (1995). The South-Pacific current. *Journal of Physical Oceanography*, *25*(1), 77–91.

van Sebille, E., England, M. H., Zika, J. D., & Sloyan, B. M. (2012). Tasman leakage in a fine-resolution ocean model. *Geophysical Research Letters*, *39*, L06601. https://doi.org/10.1029/2012GL051004

Walters, D., Baran, A. J., Boutle, I., Brooks, M., Earnshaw, P., Edwards, J., et al. (2019). The Met Office Unified Model global atmosphere 7.0/7.1 and JULES global land 7.0 configurations. *Geoscientific Model Development*, *12*(5), 1909–1963. https://doi.org/10.5194/gmd-12-1909-2019

Yool, A., Popova, E. E., & Anderson, T. R. (2013). MEDUSA-2.0: An intermediate complexity biogeochemical model of the marine carbon cycle for climate change and ocean acidification studies. *Geoscientific Model Development*, *6*(5), 1767–1811. https://doi.org/10.5194/gmd-6-1767-2013